



Ultra-trace silver-doped hydroxyapatite with non-cytotoxicity and effective antibacterial activity



Chao Shi^a, Jianyong Gao^b, Ming Wang^a, Jingke Fu^a, Dalin Wang^b, Yingchun Zhu^{a,*}

^a Key Lab of Inorganic Coating Materials, Shanghai Institute of Ceramics, Chinese Academy of Sciences, 1295 Dingxi Road, Shanghai 200050, China

^b Department of Stomatology, Changhai Hospital, Second Military Medical University, 168 Changhai Road, Shanghai 200433, China

ARTICLE INFO

Article history:

Received 28 January 2015

Received in revised form 16 April 2015

Accepted 28 May 2015

Available online xxxx

Keywords:

Ultra-trace Ag

Hydroxyapatite

Antibacterial activity

Protein adsorption

Cytotoxicity

ABSTRACT

Hydroxyapatite (HAp) nanocrystals as the main inorganic component in hard tissue have been extensively studied for bone regeneration and dental implant treatment. However, failure of surgical reconstruction often occurs owing to the lack of effective antibacterial ability of HAp. It is still a challenge to develop artificial HAp with both efficient antibacterial ability and proper biological properties. Herein, a series of ultra-trace Ag-doped HAp nanocrystals have been elaborately prepared with the optimal doping concentration from 0.27 ppm to 2.2 ppm, which present non-cytotoxicity while possess effective bacteria reduction ability. Ultra-trace Ag-doped HAp nanocrystals possess higher protein adsorption than pure HAp nanocrystals due to the trace doping-induced less negative surface potential. The ultra-trace Ag-doped HAp nanocrystals showed effectively antibacterial ability, non-cytotoxicity and enhanced adsorbability that made them ideal materials for various bio-compatible and antibacterial applications.

© 2015 Elsevier B.V. All rights reserved.

1. Introduction

Hydroxyapatite (HAp) has been extensively studied in dentistry and orthopedics due to its biocompatibility, bioactivity and osteoconductivity, which result from the structural and chemical similarities to the mineral component of mammalian bone and teeth [1–4]. As implantable biomaterials, HAp is often used as coating on metallic prostheses to improve the biological properties. It facilitates the rapid fixation and strong bonding between host bone and the implants, and accelerates uniform bone ingrowth or ongrowth at the bone-implant interface [5,6]. However, bacterial infections occur frequently after implantation in clinical due to the lack of antibacterial properties of HAp [7,8]. Once implant-associated infections occur, the pathogens aggregate rapidly and form adherent biofilms which exhibit increased protection from the host defense and enhanced resistance to antibiotic treatments [9–11]. Sometimes prosthesis removal and replacement represent the only salvage method to thoroughly eliminate severe infections, which in return will exert physical and economic stress on patients [12,13]. For this reason, effective antibacterial properties of HAp are highly desired to improve the long-time stability and performance of implantable biomaterials in dentistry and orthopedics.

In the past few years, silver has been the most stable agent to control bacteria adhesion and prevent biofilm formation for its broad antibacterial spectrum and oligodynamic bactericidal activity in different

biomedical fields [14,15]. Previous studies have revealed that silver-doped HAp has been successfully synthesized through wet chemical method and its antimicrobial behavior was studied [16–19]. Vojislav et al. prepared Ag⁺ substituted HAp nanopowders with the atomic ratio of 0.02–0.4 wt.%, which revealed 98.5%–99.7% reduction in number of viable bacteria after 4 h incubation [20]. Chuang et al. fabricated 210 ppm, 931 ppm and 10,235 ppm Ag doped HAp coatings and observed apparent inhibition zone for HAp coatings doped with 931 ppm and 10,235 ppm Ag [21]. Although Ag doped HAp can cause bacteria death enormously, high concentration of doped Ag can be toxic [22–24]. Ag concentration higher than 300 ppb in human blood can cause side-effects in the form of leukopenia, liver and kidney damage and the long-time exposure to silver exceeded the threshold limit can cause argyria to human body [25,26]. Therefore, optimization of Ag concentration in HAp is critical to guarantee Ag/HAp optimal antimicrobial ability without cytotoxicity. Based on this, our aim is to synthesize ultra-trace Ag-doped HAp that not merely develops antibacterial effect to reduce implant-associated postoperative infection, but also exhibits non-toxicity to the surrounding tissues.

In this study, a series of Ag/HAp nanocrystals with different doping ratios (0.04–197 ppm) were designed elaborately and the antibacterial effect was evaluated quantitatively against Gram-positive *Staphylococcus aureus* and Gram-negative *Escherichia coli*. The surface parameters and adsorbability related to the biomaterials-host interaction were examined in physiological environment. The HAp nanocrystals labeled with fluorescent agent were internalized into cells and the cytotoxicity was studied through cell viability evaluation. The ultra-trace Ag doped

* Corresponding author.

E-mail address: yzyhu@mail.sic.ac.cn (Y. Zhu).

HAp nanocrystals may provide new opportunities as protein transport and non-cytotoxic implant with antibacterial ability in bone tissue engineering.

2. Materials and methods

2.1. Synthesis of silver-doped hydroxyapatite

The stoichiometric HAp and Ag/HAp nanocrystals were synthesized by hydrothermal method in this article. Calcium nitrate tetrahydrate ($\text{Ca}(\text{NO}_3)_2 \cdot 4\text{H}_2\text{O}$, AR), diammonium hydrogen phosphate ($(\text{NH}_4)_2\text{HPO}_4$, AR), silver nitrate (AgNO_3 , AR) were used as the precursor without any further purification. Briefly, aqueous solutions of $\text{Ca}(\text{NO}_3)_2$ (2.8 mol/L), $(\text{NH}_4)_2\text{HPO}_4$ (0.56 mol/L) and AgNO_3 were obtained by dissolving them in deionized water. The mixed solution of $\text{Ca}(\text{NO}_3)_2$ and AgNO_3 was added dropwise to the solution of $(\text{NH}_4)_2\text{HPO}_4$. Throughout the process, the pH of suspension was maintained at 9.0 by adding ammonium hydroxide ($\text{NH}_3 \cdot \text{H}_2\text{O}$, 2 mol/L) under continuous stirring at room temperature. Then, the suspension was transferred into the reaction vessel with Teflon liner and subsequent placed in homogeneous drying oven at 150 °C for 24 h. After that, the obtained precipitate was isolated by filtration, washed with abundant deionized water for several times and dried at 80 °C. The atomic ratio of (Ag + Ca)/P in the precursor was fixed at 1.67 in all of the cases. For each sample, the varied doping concentrations were realized by changing initial concentrations of AgNO_3 precursor (from 0.1 ppm to 1000 ppm).

2.2. Characterization

The crystallinity of nanocrystals was investigated using a D/Max-2200 PC X-ray diffractometer (XRD; Rigaku, Japan) with $\text{Cu K}\alpha$ radiation ($\lambda = 1.5406 \text{ \AA}$) under 40 KV and 40 mA. The morphology and size were characterized by an S-4800 field emission scanning electron microscope (FESEM; Hitachi, Japan). Transmission electron microscope (TEM) images were obtained with a field-emission transmission electron microscope (JEOL JEM-2100 F, Japan) at an accelerating voltage of 200 kV. Samples for the investigation were prepared by ultrasonically dispersing the powders in ethanol prior to collection on a holey copper grid covered with porous carbon film. The Ag concentration of samples was determined by a 4510 Graphite furnace atomic absorption spectrophotometer (GFAAS; INESA Scientific Instrument Co. Ltd, China) with a silver hollow cathode lamp radiation ($\lambda = 328.1 \text{ nm}$) at a slit width of 0.5 nm. Specific surface areas were calculated by the Brunauer–Emmett–Teller (BET) method. All samples were pretreated for 4 h at 423 K under nitrogen before measuring on a Micrometitics Tristar 3000 system. The photoluminescence (PL) and photoluminescence excitation (PLE) of Eu/HAp were analyzed on FluoroMax®-4 fluorescence spectrometer.

2.3. Silver ion release of Ag/HAp nanocrystals

The simulated release of silver was carried out by soaking 0.5 g samples with different Ag concentration in phosphate buffer solution (PBS; 10 mL; pH 7.4). The release-medium was kept at 37 °C with shaking for 1, 3, 6, 9, 12, 24 and 48 h. Then 1 mL of Ag-released medium was extracted for subsequent GFAAS analysis and replaced with the same volume of fresh PBS, which was preheated to 37 °C.

2.4. Zeta potential measurement in different buffer solutions

The zeta potential of synthesized sample with varied Ag concentration was measured by dynamic light scattering using a Nicomp TM 380 ZLS zeta-potential/particle sizer (PSS Nicomp particle size system, USA). The powders were ultrasonically dispersed in PBS with the pH fixed at 4.5, 5.5, 6.5, 7.5 and 8.5. The zeta potential of each sample was measured 6 times and the average value was reported.

2.5. Protein adsorption assay of Ag/HAp nanocrystals against BSA

Bovine serum albumin (BSA; Sigma, purity of 99.8%) was used as model protein in this study. Initially, 10 mg of synthesized samples were ultrasonically dispersed in centrifuge tube containing 1 mL protein solution (250 $\mu\text{g}/\text{mL}$, protein/PBS), and then placed in a sterile humidified incubator at 37 °C for 4 h. The suspension was centrifuged and the amount of protein in the supernatant was measured by Micro BCA protein assay reagent kit (Pierce Biotechnology Inc.) [27]. Specifically, 25 μL protein supernatant was pipetted into a 96-well cell culture plate with 200 μL BCA working reagent in each well. The plate was mixed thoroughly on a plate shaker for 30 s, and then maintained at 37 °C for 30 min. The analysis was performed by using a micro-plate reader (Bio-Tek ELx800) at 562 nm. Each protein concentration was calibrated by a concurrently produced standard curve carried out by the same method as mentioned above. Finally, the amount of adsorbed protein on HAp or Ag/HAp was determined by subtracting the amount of protein in the corresponding supernatant.

2.6. Antibacterial activity assay

The antibacterial ability of HAp, Ag/HAp (0.04 ppm), Ag/HAp (0.27 ppm), Ag/HAp (2.2 ppm), and Ag/HAp (197 ppm) nanocrystals was evaluated by bacteriological plate counting methods using Gram-negative *Escherichia coli* (*E. coli*, ATCC25922) and Gram-positive *Staphylococcus aureus* (*S. aureus*, ATCC25923). The bacteria were cultured in liquid nutrition agar medium at 37 °C for 12 h and adjusted to a concentration of about 10^7 CFU/mL. All used laboratory supplies below were sterilized in an autoclave at 121 °C for 30 min. Briefly, 0.5 g of each sterile sample was dispersed in centrifugal tube containing PBS (9 mL) and bacteria suspension (1 mL) and incubated at 37 °C for 3, 6, 9, 12, 24, 36 and 72 h. For subsequent bacteria counting, 100 μL of suspension was extracted from centrifugal tube and inoculated into solid nutrition agar medium followed by 24 h incubation at 37 °C. The bacterial colonies were counted in accordance with the National Standard of China GB/T 4789.2 and the antibacterial rates (R%) were calculated based on the following formula:

$$R = \frac{C_t - S_t}{C_t} \times 100\%$$

where C_t represents the average number of bacteria in control group (bacteria suspension diluted by PBS without nanocrystals added in) and S_t represents the average number of bacteria in experimental group.

2.7. Cytocompatibility evaluation

2.7.1. Cell culture

In order to perform the cytocompatibility experiments, the mouse fibroblast cell line L929 (Cells Resource Center, Shanghai Institutes of Biological Science, Shanghai, P. R. China) was used according to the International Standard Organization (ISO 10993–5) protocol. Cells were cultured in RPMI 1640 medium supplemented with 2.0 g/L sodium bicarbonate, 4.5 g/L glucose, 0.11 g/L sodium pyruvate, 2.383 g/L HEPES and 10% fetal bovine serum (FBS). The cells were maintained at 37 °C in a humidified incubator under 5% CO_2 with culture medium changed every 2 days. With regard to the cell passage, all cells were harvested using 0.25% trypsin (sigma) in PBS solution (pH 7.4) and resuspended in fresh culture medium to obtain a cell monolayer suspension for further cultivation until the logarithmic phase.

2.7.2. In vitro cytotoxicity assay

MTT reduction assay was performed to evaluate the in vitro cytotoxicity of Ag/HAp nanocrystals. For each sterile sample, series of suspension (50 $\mu\text{g}/\text{mL}$, 200 $\mu\text{g}/\text{mL}$, 500 $\mu\text{g}/\text{mL}$ and 1000 $\mu\text{g}/\text{mL}$) were prepared by dispersing nanocrystals into RPMI 1640 medium culture,

respectively. Firstly, 150 μL of cell suspension with a density of 6.0×10^4 cells/mL was seeded in 96-well plates and cultured for 24 h. Then, the culture medium was removed followed by washing with PBS and replaced by 150 μL nanocrystals suspension with different concentrations. In blank control group, 150 μL RPMI 1640 medium with 10% FBS was added in corresponding wells. After 24 h incubation, the culture medium was removed and washed twice with PBS to remove residual nanoparticles. Then, 20 μL of 5 mg/mL 3-(4,5-dimethylthiazol-2-yl)-2,5-diphenyl tetrazolium bromide (MTT) solution was added into each well. After additional 4 h incubation, MTT solution was replaced with dimethylsulfoxide (DMSO, 150 μL per well). After shaking for 10 min, the optical density (OD) was measured using a micro-plate reader (Bio-Tek ELx800) at 490 nm.

2.7.3. Cellular uptake of fluorescently labeled HAp nanocrystals

Eu/HAp nanocrystals were synthesized as photoluminescence agent using the same method mentioned above. For fluorescence microscopy observations, L929 cells were seeded in 35 mm petri-dishes and incubated with Eu/HAp nanocrystals suspension ultrasonically dispersed previously. After 24 h incubation, the medium was removed and the cells were washed thrice with PBS to remove residual nanocrystals. Then, 1 mL of PBS was added and the cells were visualized through inverted fluorescence microscope (Olympus IX71, Japan).

2.8. Statistical analysis

All the data were collected in independent triplicate experiments and expressed as means \pm standard deviation ($n = 6$). Statistically significant differences (p) between the various groups were measured using one-way analysis of variance and Tukey's multiple comparison tests.

3. Results and discussion

3.1. Characterization of silver-doped hydroxyapatite

Five HAp samples were prepared with different Ag doping concentration of 0 ppm, 0.04 ppm, 0.27 ppm, 2.2 ppm and 197 ppm. Table 1 lists Ag concentration and doping ratio of obtained Ag/HAp products. It can be found that doping ratio decreased from 80% to 51% when Ag doping concentration increased from 0.04 ppm to 197 ppm. It can be explained by the lattice distortion of Ag/HAp nanocrystals due to the differences in ionic radius between Ag^+ and Ca^{2+} [28]. When more Ag^+ substituted Ca^{2+} in HAp, larger lattice distortion will impede further substitution which leads to the decrease of doping ratio.

The XRD patterns of un-doped and Ag doped HAp nanocrystals were shown in Fig. 1. All patterns exhibited pure HAp phase (JCPDS 09-0432) and the sharp diffraction peaks indicated that HAp nanocrystals were well crystallized. Compared with un-doped HAp nanocrystals, no new peaks appeared for Ag doped HAp samples even the doping concentration increased to 197 ppm (i.e. the mole ratio of $\text{Ag}/(\text{Ag} + \text{Ca})$ is 0.18%). It was suggested that Ag^+ has been incorporated into HAp lattice in the way of substituting Ca^{2+} in the present work.

The morphologies of as-prepared un-doped and Ag doped HAp nanocrystals were examined by SEM and TEM (Fig. 2). The samples

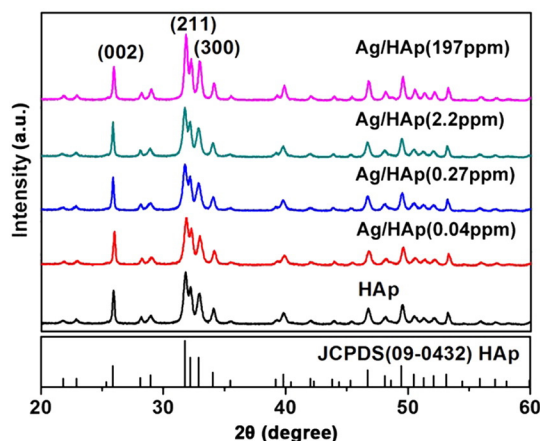


Fig. 1. The XRD patterns of HAp nanocrystals doped with different Ag concentration.

were nanorod-like particles with a length of 100–250 nm and a diameter of ca. 20 nm, which has gained much attention due to the good adsorbability on various proteins [29]. The average length of Ag doped HAp nanorods increased from 128 nm to 248 nm when Ag doping concentration increased from 0.04 ppm to 197 ppm. The ionic radius and electronegativity of Ag^+ are larger than Ca^{2+} , which may facilitate the crystal growth of HAp nanocrystals [30,31]. From TEM and HRTEM images of sample Ag/HAp (0.27 ppm) (Fig. 2d), it shows that the Ag/HAp nanocrystals exhibit clear and homogeneous surface morphology (see TEM image) and distinct lattice fringes (see HRTEM image inserted in Fig. 2d) without the existence of Ag nanoparticles and Ag layer on surface of Ag/HAp nanocrystals. The Ag^+ in precursor solution has been successfully entrapped in HAp lattice in the method of substituting Ca^{2+} .

3.2. Silver ion release of Ag/HAp nanocrystals

Fig. 3a–b displays the time dependency and concentration dependency of Ag^+ -release profiles for different concentration Ag doped HAp nanocrystals as a function of immersion time. Initially, a fast release of Ag^+ was observed for all tested samples in the first 12 h of immersion. In the following 36 h of continuous immersion, the release gradually decreased and achieved the maximum concentration at 48 h in all curves. Generally, increasing amount of Ag doped in HAp nanocrystals definitely lead to high concentration of released Ag^+ . Sample Ag/HAp (197 ppm) released the highest amount of 1900 ppb Ag^+ after 48 h immersion in PBS, compared with 46 ppb, 11 ppb and 2 ppb for samples Ag/HAp (2.2 ppm), Ag/HAp (0.27 ppm) and Ag/HAp (0.04 ppm). Considering the cytotoxicity of Ag^+ , an optimum concentration of released Ag^+ should be controlled to minimize potential side-effects. In this study, the Ag^+ released from all Ag/HAp samples except Ag/HAp (197 ppm) was lower than the maximum toxic concentration (300 ppb) in human blood, indicating the possibility to be non-cytotoxic biomaterials [26].

Table 1

List of Ag/HAp nanocrystals with different Ag doping concentration and doping ratio.

Samples	Initial concentration of Ag (ppm)	Doping concentration of Ag (ppm)	Doping ratio (%)
HAp	0	0	–
Ag/HAp (0.04 ppm)	0.05	0.04 ± 0.01	80%
Ag/HAp (0.27 ppm)	0.38	0.27 ± 0.02	71%
Ag/HAp (2.2 ppm)	3.84	2.20 ± 0.2	57%
Ag/HAp (197 ppm)	384	197 ± 2.5	51%

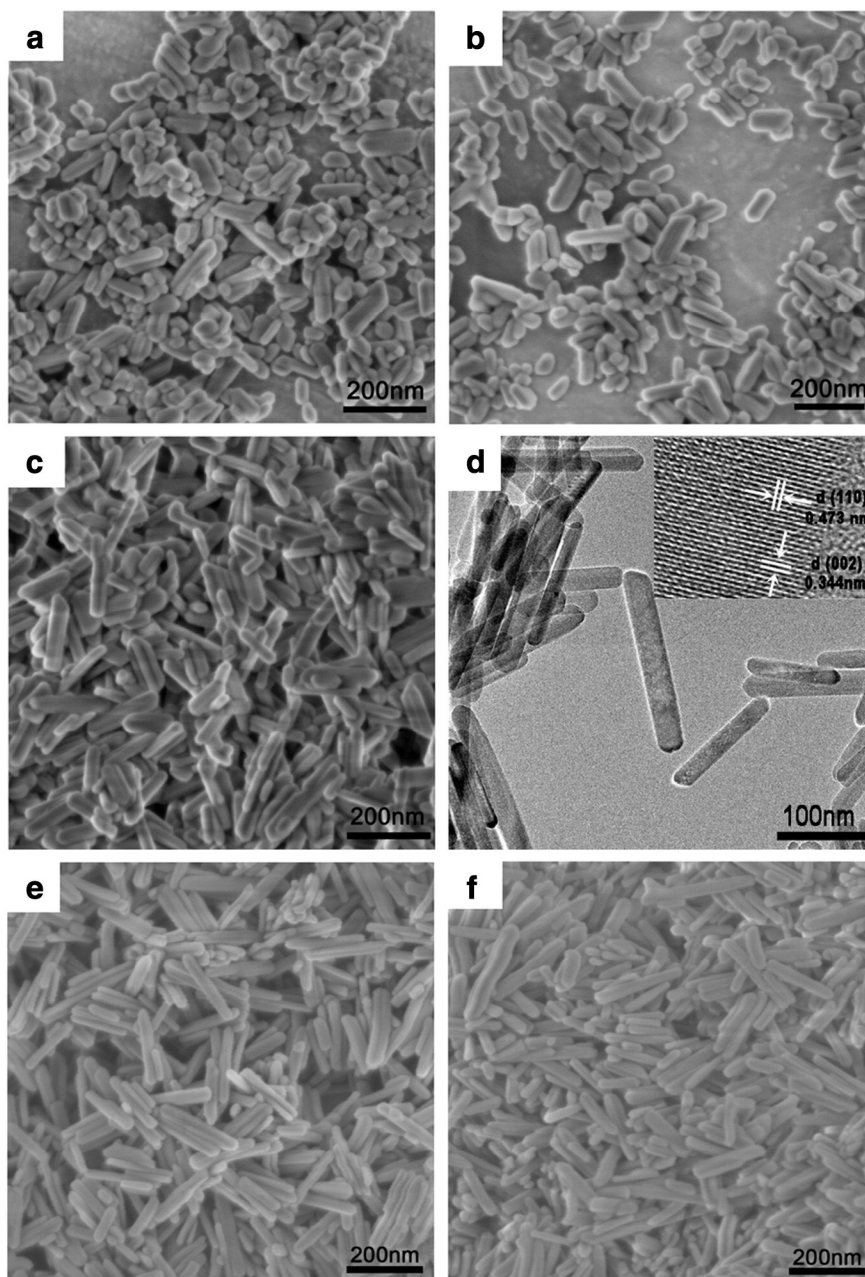


Fig. 2. (a–f) SEM and TEM images of un-doped and Ag doped HAp nanocrystals (a) HAp, (b) Ag/HAP (0.04 ppm), (c–d) Ag/HAP (0.27 ppm), (e) Ag/HAP (2.2 ppm) and (f) Ag/HAP (197 ppm).

3.3. Zeta potential and protein adsorption analysis

Fig. 4a shows zeta potentials of un-doped and Ag doped HAp nanocrystals as a function of pH of the buffer solutions. It shows that all samples exhibited negative zeta potential between -3.66 mV and -29.3 mV. This is due to the chemicals involved in the synthesis process, in which ammonia solution was added to keep the suspension alkaline [32]. The zeta potential in all curves exhibits a downward trend with the upward of pH values in PBS, which results from the aggregation of negative charges inside the electric double layer (EDL). Compared with un-doped HAp nanocrystals, the zeta potential of Ag doped HAp becomes less negative and the tendency becomes obvious as increasing the Ag doping concentration. Sample Ag/HAP (197 ppm) exhibits a zeta potential of -21.4 mV while that is -25.7 mV for HAp at pH 7.5. It can be ascribed to the variation of divalent calcium ions

(Ca^{2+}) in the “calcium-rich layer” formed by initial dissolution of a small portion of HAp (Fig. 4b) [33,34]. When divalent Ca^{2+} ions were replaced by monovalent Ag^+ ions, the number of net positive charge existed in “calcium-rich layer” became less, leading to less anion attracted to the electric double layer, and a shift toward positive values appears consequently for Ag doped HAp nanocrystals.

As the initial response of extracellular matrix to biomaterials, the protein adsorption of Ag/HAP was conducted under physiological condition (pH 7.4). The results of bovine serum albumin (BSA) adsorption on un-doped and Ag doped HAp nanocrystals at pH 7.4 are shown in Fig. 5. It can be found that Ag/HAP (0.27 ppm) exhibits the maximum adsorption (16.7 $\mu\text{g}/\text{mg}$) among these five samples. The amount of adsorbed BSA increases when Ag concentration increases from 0.04 ppm to 0.27 ppm, but decreases when the concentration increases to 2.2 ppm and 197 ppm.

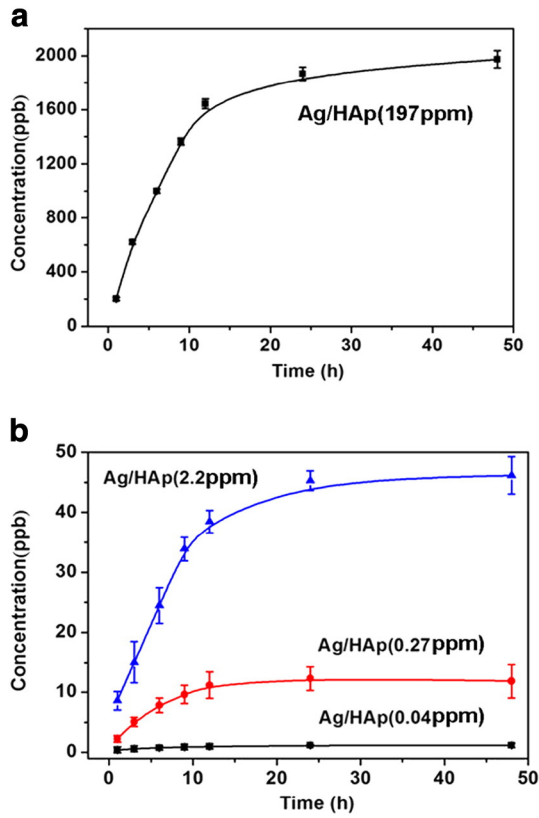


Fig. 3. In vitro Ag^+ -release profiles of Ag doped HAp nanocrystals at different immersion times in PBS solution.

Generally, the interactions between biomolecules and materials are dynamic and complex, which relate to physical and chemical properties of materials as well as intrinsic properties of proteins in the medium [35, 36]. In this study, the differences in the capacity of binding protein are attributed to a synergistic effect of surface charges and specific surface area of nanocrystals. It should be noted that the BSA protein (pI 4.7) will be negatively charged in PBS with physiological pH 7.4. When more Ag was doped into HAp nanocrystals, the less negative zeta potential weakened the electrostatic repulsion between Ag doped HAp and negatively charged BSA, resulting in more protein adsorbed on surface of Ag/HAp (0.27 ppm) compared with HAp and Ag/HAp (0.04 ppm). However, when the Ag doping concentration was further enhanced from 0.27 ppm to 197 ppm, the specific surface area of nanocrystals varied from $32.42 \text{ m}^2/\text{g}$ to $16.21 \text{ m}^2/\text{g}$ (Table S1) and the protein binding sites may be insufficient to provide the location of BSA protein. As a result, Ag/HAp (2.2 ppm) and Ag/HAp (197 ppm) exhibited a downward trend of protein adsorption compared to Ag/HAp (0.27 ppm).

3.4. Antibacterial activity evaluation of Ag/HAp nanocrystals

In order to evaluate the bactericidal effect, the bacteria were cultivated with various nanocrystals for a series of time and re-cultivated on agar according to the bacteria counting method. The viable bacteria number curves and bacteria reduction percentage for *E. coli* and *S. aureus* as a function of time are depicted in Fig. 6. The proliferation of bacteria is reduced sharply in Ag doped HAp groups compared with blank and HAp groups, implying the apparent bacteriostatic effect on both *E. coli* and *S. aureus* (Fig. 6a, c). The bacterium reduction of Ag/HAp nanocrystals exhibit dose- and time-dependent features (Fig. 6b, d). The antibacterial rates of Ag/HAp (0.04 ppm) are enhanced from 40% to 63% when the incubation time extended from 3 h to 72 h. Moreover, the antibacterial rate increases from 63% to 99% after 24 h incubation when the Ag doping concentration is enhanced from 0.04 ppm to

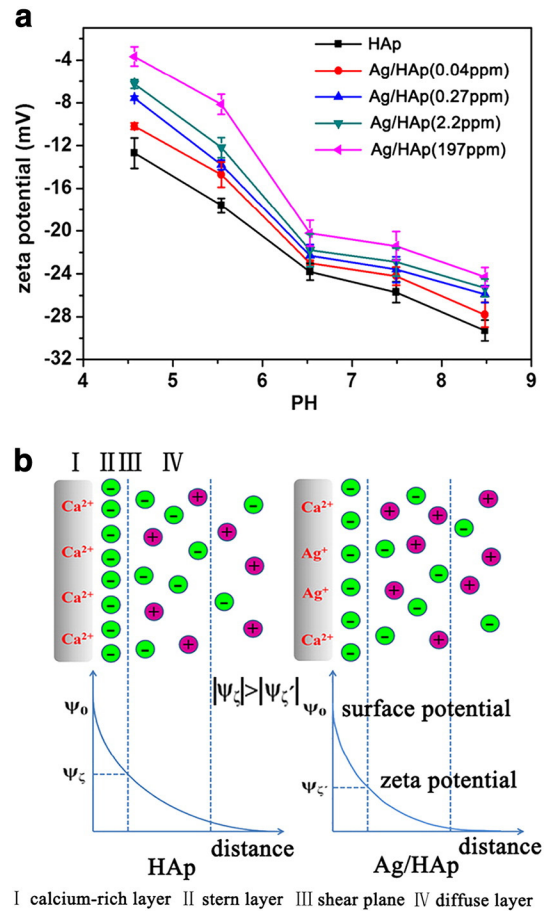


Fig. 4. (a) The zeta potential of un-doped and Ag doped HAp nanocrystals as a function of pH in PBS. (b) The corresponding model of electric double layer for HAp and Ag doped HAp nanocrystals immersed in PBS. Briefly, less negative charges accumulated around the Ag doped HAp nanocrystals in stern layer compared with HAp nanocrystals when the Ca^{2+} was partially substituted by Ag^+ . And zeta potential at shear plane shifted toward positive values consequently.

197 ppm. According to the National Standard of China GB/T 20944.3 protocol, the effective antibacterial ability is defined as a percentage of bacteria reduction above 70% for *E. coli* and *S. aureus*. The antibacterial

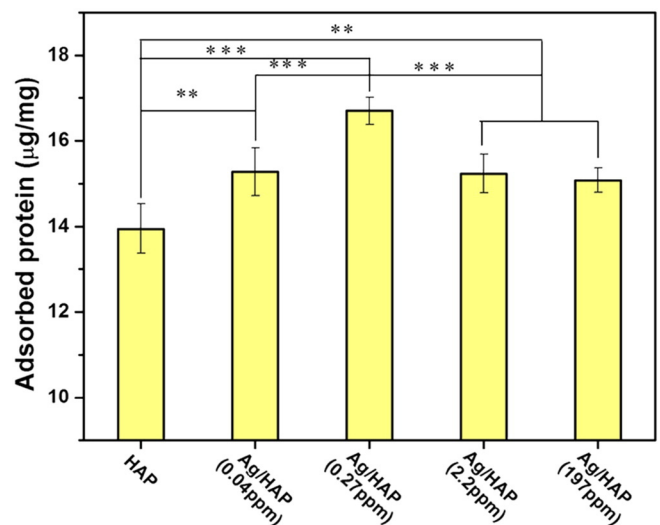


Fig. 5. The protein adsorption histogram of BSA on un-doped and Ag doped HAp nanocrystals.

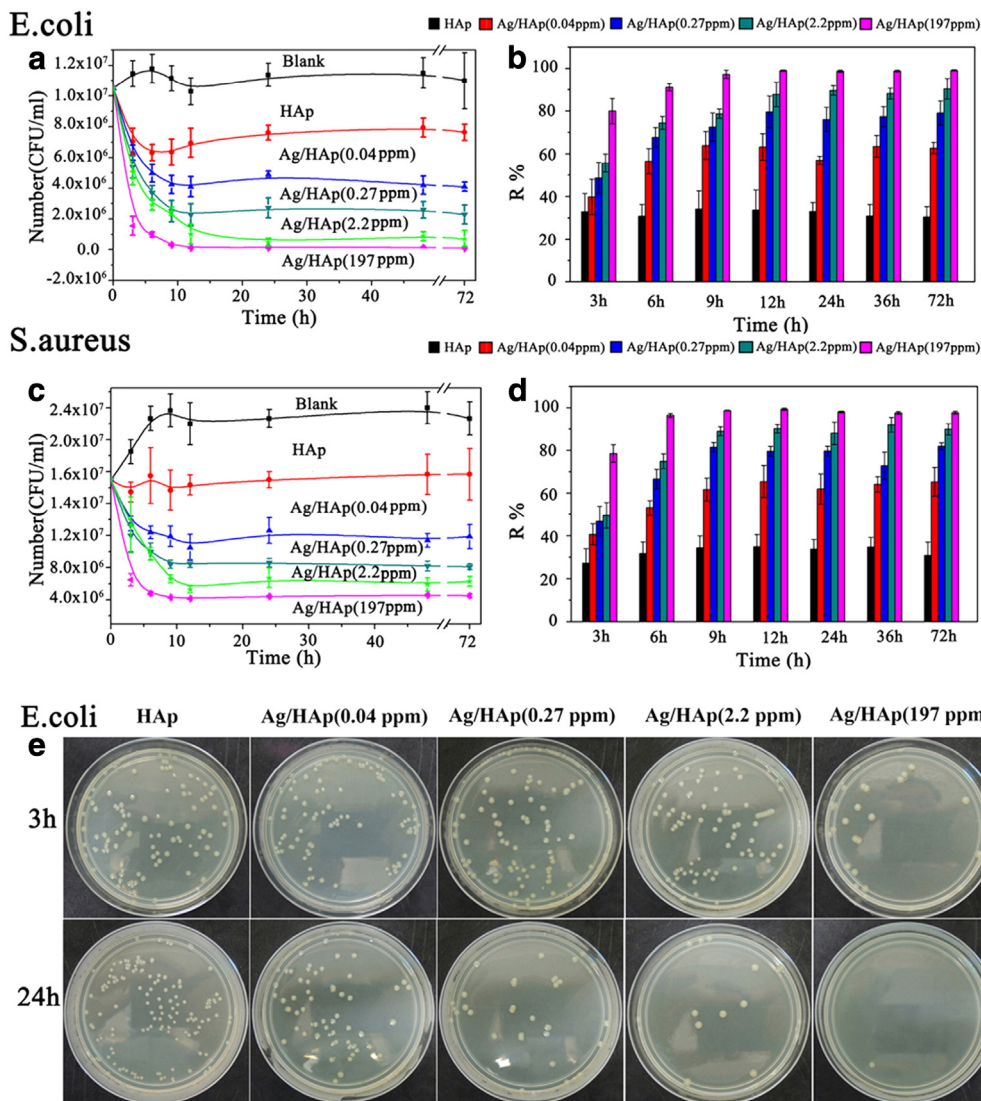


Fig. 6. The viable bacteria number curves (a, c) and percentage of bacteria reduction (b, d) for *E. coli* (a, b) and *S. aureus* (c, d) treated with HAp and Ag doped HAp nanocrystals as a function of time. (e) Typical photographs of re-cultivated *E. coli* colonies on agar for 3 h and 24 h with 10,000-fold dilution. All the data were presented as means \pm SDs ($n = 6$) and exhibited a significant difference compared with that of HAp. The bacteria reduction (either *E. coli* or *S. aureus*) exhibited a dose- and time-dependent phenomenon.

results show that the antibacterial rates are 82% and 90% when 0.27 ppm and 2.2 ppm Ag are doped in HAp nanocrystals, respectively. Ag/HAp (2.2 ppm) exhibits effective antibacterial ability with 46 ppb Ag^+ released in solution, which is lower than the 50 ppb limit concentration of Ag^+ in drinking-water published by WHO. The maximum Ag content that exhibits effective antibacterial and non-cytotoxic may be 2.2 ppm. The effective antibacterial activity of ultra-trace Ag doped HAp reveals that high doping concentration of Ag is not necessary to achieve effective antibacterial activity for HAp, appropriate amount of ultra-trace doping can also be adopted as an ideal option.

The viability of microorganism can be affected by physical and chemical characteristics of surrounding materials, including morphology, surface properties and chemical composition [37,38]. It has been demonstrated that nanoparticles showed toxicity to test bacteria partially due to their greater tendency to attach to the cell walls than to aggregate together [39]. And the smaller size (diameter) of nanomaterials, the more toxic occurs to bacteria. In this study, the synthesized samples exhibit a homogeneous nanorod-like structure with a high specific surface area, which contributes to the antibacterial activity through undermining cell membrane of bacteria. It can be verified by HAp

group in this test that also shows slightly bacteria reduction which can be ascribed to the direct contact of microorganism to HAp nanocrystals.

As for the mechanism of the antibacterial activity of Ag/HAp, it is widely accepted that the broad-spectrum of antimicrobial activity is resulted from the release of Ag^+ [40]. Previous studies have revealed that the released Ag^+ will bind to proteins on the membrane, thereby causing structural changes and damage to the membranes [41]. Then, Ag^+ penetrates into cells and interacts with nucleic acids, preventing proliferation process and causing bacteria death [42]. Previous reports revealed that effective antibacterial activity can be obtained when Ag^+ concentration reaches as high as 35 ppb [43,44]. For Ag/HAp (2.2 ppm) and Ag/HAp (197 ppm), the bacteria were 90% and 99% reduced with the accumulated Ag^+ -release amount (46 ppb, 1900 ppb) higher than 35 ppb. However, the ultra-trace Ag/HAp (0.27 ppm) also exhibited 82% bacteria reduction with only 11 ppb Ag^+ release. It may be due to the contact antibacterial process that causes bacteria death at the surface of Ag/HAp nanoparticles. The positive charged Ag^+ tends to aggregated at surface of Ag/HAp nanocrystals due to negative zeta potential as EDL theory described, which lead to higher concentration of Ag^+ at Ag/HAp surface than that detected in the interior of the

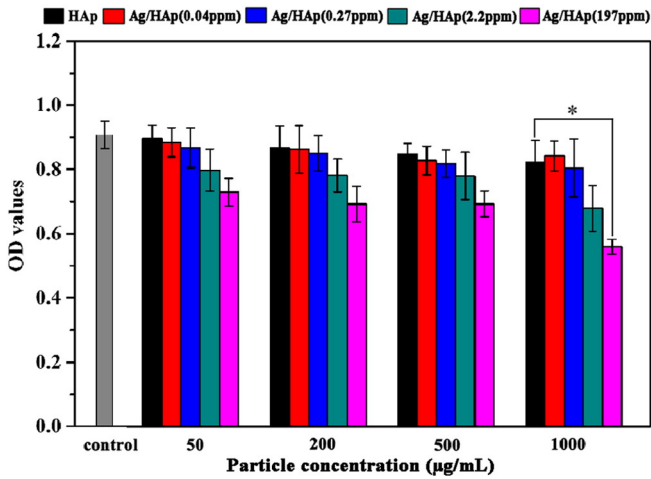


Fig. 7. In vitro cytocompatibility assay of Ag/HAp nanocrystals against L929 cells after co-incubation for 24 h. The OD values directly proportional to cell viability was determined with regard to the concentration of nanoparticles (50–1000 µg/mL). All the data exhibited a downward trend as the increasing concentration of either un-doped or Ag doped HAp nanoparticles. No significant differences were founded in ultra-trace Ag/HAp (0.04 ppm, 0.27 ppm, 2.2 ppm) groups compared with blank control group. However, Ag/HAp (197 ppm, 1000 µg/mL) group exhibited certain cytotoxicity with only 62% cell viability when compared with blank control group (* $P < 0.05$, $n = 6$).

solution. When the bacteria contact Ag/HAp nanoparticles, the bacteria were killed due to the high concentration of Ag^+ at Ag/HAp surface.

3.5. In vitro cytotoxicity of Ag/HAp nanocrystals

The in vitro cytotoxicity of antibacterial Ag/HAp nanocrystals was investigated through cell viability evaluation using mouse fibroblast

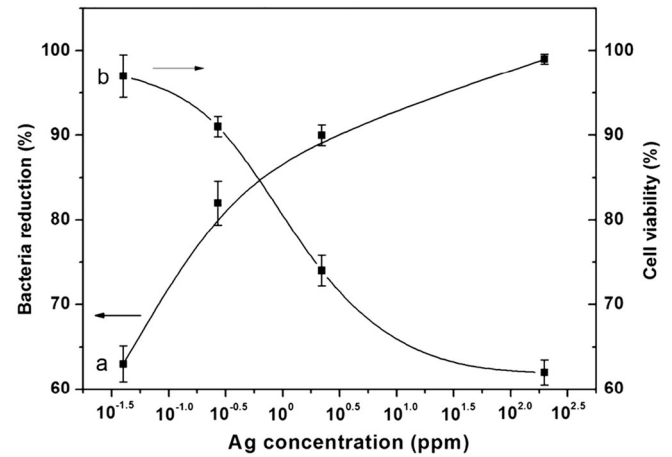


Fig. 9. The antibacterial ability and cytocompatibility assay in vitro for Ag/HAp nanocrystals with different Ag doping concentration. (a): The data represented antibacterial ratio of various Ag/HAp samples for *E. coli* at 24 h. (b): The data were calculated by comparing the OD values of experimental groups with blank control group in the case of 1000 µg/mL. The bacteria reduction and cell viability showed upward and downward trend as the increasing Ag concentration. An intersection of the two curves appears between 0.27 ppm and 2.2 ppm where Ag/HAp may nanocrystals exhibit optimal biological effects.

cell line (L929) advised by ISO 10993–5:2009 and the results are shown in Fig. 7. The results show that the cell viability is affected to some extent in a broad concentration (50–1000 µg/mL) of each sample. All five groups of L929 cells show decreased cell viability with increasing the concentration of treated Ag/HAp nanocrystals, indicating that the inhibition of cell proliferation is dose-dependent. Moreover, the cell viability is reduced gradually as the

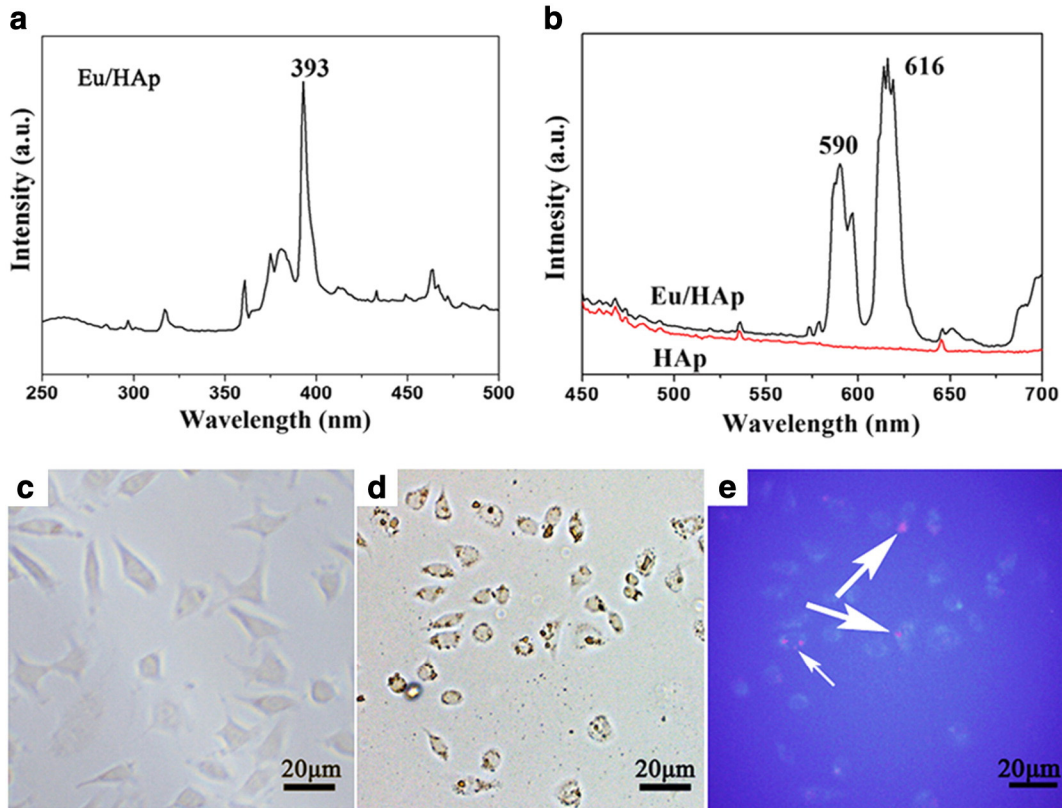


Fig. 8. Room-temperature (a) excitation spectrum and (b) PL emission spectra of Eu/HAp nanocrystals. In vitro microscopic images of L929 cells (c) before and (d) 24 h after co-incubating with Eu/HAp nanocrystals. (e) And the corresponding fluorescence image of L929 cells with UV excitation. The orange-red color located in cells was indicated by the arrow. (For interpretation of the references to color in this figure legend, the reader is referred to the web version of this article.)

increase of Ag doping concentration for any treated concentration of nanocrystals. For sample Ag/HAp (197 ppm), the viability of cells cultured with 50 $\mu\text{g}/\text{mL}$ nanoparticles is slightly affected compared with control group, whereas the cell viability significantly decreases about 40% when cultured with 1000 $\mu\text{g}/\text{mL}$ nanoparticles, which suggests that the high doping amount of Ag definitely show toxicity on cells. For ultra-trace doped Ag/HAp (0.04 ppm), Ag/HAp (0.27 ppm) and Ag/HAp (2.2 ppm) nanocrystals, the OD values display no significant differences compared with blank control group, showing no cytotoxicity on L929 cells at a large range of concentration (50–1000 $\mu\text{g}/\text{mL}$).

3.6. Cellular uptake of cationic doped HAp nanocrystals

To examine the cell-uptake property of HAp nanocrystals, Eu doped HAp (Eu/HAp) was obtained through the same hydrothermal method for fluorescence labeling. For nanocrystals-cell system, the cellular uptake is generally size-dependent for special nanocrystals [45,46]. The Eu and Ag doped HAp nanocrystals have similar morphology and particle size (Fig. S1). Fig. 8a–b shows PL excitation and emission spectra of Eu/HAp nanoparticles measured at room temperature. The most intense excitation peak of Eu/HAp nanoparticles is located at 393 nm and the two orange-red light emission peaks at 590 nm and 616 nm corresponds to the ${}^5\text{D}_0 \rightarrow {}^7\text{F}_1$ and ${}^5\text{D}_0 \rightarrow {}^7\text{F}_2$ transition within Eu^{3+} , respectively [47]. After incubation for 24 h, Eu/HAp nanoparticles were mainly located in the cytoplasm or around cell membrane region (Fig. 8d). The orange-red color was observed in corresponding fluorescence image shown in Fig. 8e, indicating Eu/HAp nanocrystals were internalized by L929.

Although it has been identified that the antibacterial properties of Ag were dose-dependent [21,48], high concentrations of Ag have been reported to be cytotoxic [22,49]. Therefore, appropriate doping concentration that possesses considerable antibacterial ability as well as non-cytotoxicity will be delicate choice in fabrication of Ag doped HAp implant. Fig. 9 depicted the curves of bacteria reduction and cell viability in vitro of all five samples as a function of Ag concentration. The bacteria reduction showed a downward trend with increasing Ag concentration while the cell viability exhibited an upward trend. When the Ag concentration is 0.04 ppm (i.e. $10^{-1.4}$ ppm), high cytocompatibility was observed with 97% cell viability accompanied by 63% antibacterial ratio. When the Ag concentration was enhanced to 0.27 ppm (i.e. $10^{-0.57}$ ppm), the antibacterial ratio was greatly improved to 82% while the cell viability was reduced to 91%. Upon further adding the doping concentration (2.2 ppm, i.e. $10^{0.34}$ ppm), the antibacterial activity was enhanced unceasingly to 90% with 74% cell viability. When Ag concentration comes to 197 ppm (i.e. $10^{2.3}$ ppm), 99% of bacteria were killed while the cytotoxicity also becomes serious with only 62% cell viability. The two curves come into an intersection between 0.27 ppm and 2.2 ppm Ag doped HAp, which exhibited 85% antibacterial activity and 85% cell viability. Ag/HAp nanocrystals with doping amount at this point may be an optimal choice for the biological effects evaluation.

4. Conclusions

In conclusion, our studies demonstrate that HAp nanocrystals doped with ultra-trace Ag possess effective antibacterial activity and non-cytotoxicity. The antibacterial rate increases from 63% to 99% while the cell viability decreases from 97% to 62% when the Ag-doping concentration varies from 0.04 to 197 ppm. The optimal properties with excellent cytocompatibility and antibacterial ability can be achieved when the Ag-doping concentration is between 0.27 ppm and 2.2 ppm. The antibacterial HAp with ultra-trace Ag is non-toxicity to living cells and tissues even if the particles are internalized by cells. The protein adsorbability of Ag/HAp can also be enhanced compared with HAp

nanocrystals due to the trace doping-induced less negative surface potential. Taken together, ultra-trace Ag doped HAp nanocrystals are potentially applicable as growth factor transporter and bone substitution materials in tissue engineering.

Acknowledgments

We gratefully acknowledge the financial support by the National Natural Science Foundation of China (Nos. 51072217, 51232007, 51132009); the Science and Technology Commission of Shanghai Municipality: (11XD1405600).

Appendix A. Supplementary data

Supplementary data to this article can be found online at <http://dx.doi.org/10.1016/j.msec.2015.05.078>.

References

- [1] R.Z. LeGeros, Calcium phosphate-based osteoinductive materials, *Chem. Rev.* 108 (2008) 4742–4753.
- [2] S.V. Dorozhkin, M. Epple, Biological and medical significance of calcium phosphates, *Angew. Chem. Int. Ed.* 41 (2002) 3130–3146.
- [3] H.Q. Cao, L. Zhang, H. Zheng, Z. Wang, Hydroxyapatite nanocrystals for biomedical applications, *J. Phys. Chem. C* 114 (2010) 18352–18357.
- [4] E.S. Ahn, N.J. Gleason, A. Nakahira, J.Y. Ying, Nanostructure processing of hydroxyapatite-based bioceramics, *Nano Lett.* 1 (2001) 149–153.
- [5] L. Sun, C.C. Berndt, K.A. Gross, A. Kucuk, Material fundamentals and clinical performance of plasma-sprayed hydroxyapatite coatings: a review, *J. Biomed. Mater. Res.* 58 (2001) 570–592.
- [6] Y. Huang, Y. Qu, B.C. Yang, W. Li, B. Zhang, X.D. Zhang, In vivo biological responses of plasma sprayed hydroxyapatite coatings with an electric polarized treatment in alkaline solution, *Mater. Sci. Eng. C* 29 (2009) 2411–2416.
- [7] A. Simchi, E. Tamjid, F. Pishbin, A.R. Boccacini, Recent progress in inorganic and composite coatings with bactericidal capability for orthopaedic applications, *Nanomedicine: NBM* 7 (2011) 22–39.
- [8] J. Esteban, J. Cordero-Ampuero, Treatment of prosthetic osteoarthritic infections, *Expert. Opin. Pharmacother.* 12 (2011) 899–912.
- [9] D. Campoccia, L. Montanaro, C.R. Arciola, The significance of infection related to orthopedic devices and issues of antibiotic resistance, *Biomaterials* 27 (2006) 2331–2339.
- [10] J.W. Costerton, P.S. Stewart, E.P. Greenberg, Bacterial biofilms: a common cause of persistent infections, *Science* 284 (1999) 1318–1322.
- [11] Y.K. Chen, X.B. Zheng, Y.T. Xie, C.X. Ding, H.J. Ruan, C.Y. Fan, Anti-bacterial and cytotoxic properties of plasma sprayed silver-containing HA coatings, *J. Mater. Sci. Mater. Med.* 19 (2008) 3603–3609.
- [12] E.M. Hetrick, M.H. Schoenfish, Reducing implant-related infections: active release strategies, *Chem. Soc. Rev.* 35 (2006) 780–789.
- [13] C.R. Arciola, D. Campoccia, P. Speziale, L. Montanaro, J.W. Costerton, Biofilm formation in Staphylococcus implant infections. A review of molecular mechanisms and implications for biofilm-resistant materials, *Biomaterials* 33 (2012) 5967–5982.
- [14] Q.L. Feng, F.Z. Cui, T.N. Kim, J.W. Kim, Ag-substituted hydroxyapatite coatings with both antimicrobial effects and biocompatibility, *J. Mater. Sci. Lett.* 18 (1999) 559–561.
- [15] B. Singh, A.K. Dubey, S. Kumar, N. Saha, B. Basu, R. Gupta, In vitro biocompatibility and antimicrobial activity of wet chemically prepared $\text{Ca}_{10-x}\text{Ag}_x(\text{PO}_4)_6(\text{OH})_2$ ($0.0 \leq x \leq 0.5$) hydroxyapatites, *Mater. Sci. Eng. C* 31 (2011) 1320–1329.
- [16] T.N. Kim, Q.L. Feng, J.O. Kim, J. Wu, H. Wang, G.Q. Chen, F.Z. Cui, Antimicrobial effects of metal ions (Ag⁺, Cu²⁺, Zn²⁺) in hydroxyapatite, *J. Mater. Sci. Mater. Med.* 9 (1998) 129–134.
- [17] K.S. Oh, S.H. Park, Y.K. Jeong, Antimicrobial effects of Ag doped hydroxyapatite synthesized from co-precipitation route, *Key Eng. Mater.* 264–268 (2004) 2111–2114.
- [18] N. Rameshbabu, T.S.S. Kumar, T.G. Prabhakar, V.S. Sastry, K.V.G.K. Murty, K.P. Rao, Antibacterial nanosized silver substituted hydroxyapatite: synthesis and characterization, *J. Biomed. Mater. Res.* 80A (2007) 581–591.
- [19] Y. Ando, H. Miyamoto, I. Noda, N. Sakurai, T. Akiyama, Y. Yonekura, T. Shimazaki, M. Miyazaki, M. Mawatari, T. Hotokebuchi, Calcium phosphate coating containing silver shows high antibacterial activity and low cytotoxicity and inhibits bacterial adhesion, *Mater. Sci. Eng. C* 30 (2010) 175–180.
- [20] V. Stanić, D. Janačković, S. Dimitrijević, S.B. Tanasković, M. Mitrić, M.S. Pavlović, A. Krstić, D. Jovanović, S. Raičević, Synthesis of antimicrobial monophase silver-doped hydroxyapatite nanopowders for bone tissue engineering, *Appl. Surf. Sci.* 257 (2011) 4510–4518.
- [21] R.J. Chung, M.F. Hsieh, C.W. Huang, L.H. Perng, H.W. Wen, T.S. Chin, Antimicrobial effects and human gingival biocompatibility of hydroxyapatite sol–gel coatings, *J. Biomed. Mater. Res.* 76B (2006) 169–178.
- [22] M. Roy, G.A. Fielding, H. Beyenal, A. Bandyopadhyay, S. Bose, Mechanical, in vitro antimicrobial, and biological properties of plasma-sprayed silver-doped hydroxyapatite coating, *ACS Appl. Mater. Interfaces* 4 (2012) 1341–1349.

- [23] B. Baruwati, S.O. Simmons, R.S. Varma, B. Veronesi, "Green" synthesized and coated nanosilver alters the membrane permeability of barrier (intestinal, brain endothelial) cells and stimulates oxidative stress pathways in neurons, *ACS Sustainable Chem. Eng.* 1 (2013) 753–759.
- [24] K. Jamuna-Thevi, S.A. Bakar, S. Ibrahim, N. Shahab, M.R.M. Toff, Quantification of silver ion release, in vitro cytotoxicity and antibacterial properties of nanostructured Ag doped TiO₂ coatings on stainless steel deposited by RF magnetron sputtering, *Vacuum* 86 (2011) 235–241.
- [25] S. Maitre, K. Jaber, J.L. Perrot, C. Guy, F. Cambazard, Increased serum and urinary levels of silver during treatment with topical silver sulfadiazine, *Ann. Dermatol. Venerol.* 129 (2002) 217–219.
- [26] J. Hardes, H. Ahrens, C. Gebert, A. Streitburger, H. Buerger, M. Erren, A. Günsel, C. Wedemeyer, G. Saxler, W. Winkelmann, G. Gosheger, Lack of toxicological side-effects in silver-coated megaprotheses in humans, *Biomaterials* 28 (2007) 2869–2875.
- [27] X.F. Niu, Q.L. Feng, M.B. Wang, X.D. Guo, Q.X. Zheng, Porous nano-HA/collagen/PLLA scaffold containing chitosan microspheres for controlled delivery of synthetic peptide derived from BMP-2, *J. Control. Release* 134 (2009) 111–117.
- [28] S. Samani, S.M. Hossainipour, M. Tamizifar, H.R. Rezaie, In vitro antibacterial evaluation of sol–gel-derived Zn-, Ag-, and (Zn plus Ag)-doped hydroxyapatite coatings against methicillin-resistant *Staphylococcus aureus*, *J. Biomed. Mater. Res.* 101 (2013) 222–230.
- [29] M. Zandi, H. Mirzadeh, C. Mayer, H. Urch, M.B. Eslaminejad, F. Bagheri, H. Mivehchi, Biocompatibility evaluation of nano-rod hydroxyapatite/gelatin coated with nano-HAp as a novel scaffold using mesenchymal stem cells, *J. Biomed. Mater. Res.* 92A (2010) 1244–1255.
- [30] K.J. Zhu, K. Yanagisawa, R. Shimanouchi, A. Onda, K. Kajiyoshi, Preferential occupancy of metal ions in the hydroxyapatite solid solutions synthesized by hydrothermal method, *J. Eur. Ceram. Soc.* 26 (2006) 509–513.
- [31] F. Chen, P. Huang, Y.J. Zhu, J. Wu, C.L. Zhang, D.X. Cui, The photoluminescence, drug delivery and imaging properties of multifunctional Eu³⁺/Gd³⁺ dual-doped hydroxyapatite nanorods, *Biomaterials* 32 (2011) 9031–9039.
- [32] S. Patil, A. Sandberg, E. Heckert, W. Self, S. Seal, Protein adsorption and cellular uptake of cerium oxide nanoparticles as a function of zeta potential, *Biomaterials* 28 (2007) 4600–4607.
- [33] K. Cheng, W. Weng, H. Wang, S. Zhang, In vitro behavior of osteoblast-like cells on fluoridated hydroxyapatite coatings, *Biomaterials* 26 (2005) 6288–6295.
- [34] P.W. Brown, R.I. Martin, An analysis of hydroxyapatite surface layer formation, *J. Phys. Chem. B* 103 (1999) 1671–1675.
- [35] W. Pon-On, N. Charoenphandhu, J. Teerapornpantakit, J. Thongbunchoo, N. Krishnamra, I.M. Tang, Physicochemical and biochemical properties of iron-loaded silicon substituted hydroxyapatite (FeSiHAp), *Mater. Chem. Phys.* 141 (2013) 850–860.
- [36] K. Kandori, T. Kuroda, S. Togashi, E. Katayama, Preparation of calcium hydroxyapatite nanoparticles using microreactor and their characteristics of protein adsorption, *J. Phys. Chem. B* 115 (2011) 653–659.
- [37] A. Simon-Deckers, S. Loo, M. Mayne-L'Hermite, N. Herlin-Boime, N. Menguy, C. Reynaud, B. Gouget, M. Carriere, Size-, composition- and shape-dependent toxicological impact of metal oxide nanoparticles and carbon nanotubes toward bacteria, *Environ. Sci. Technol.* 43 (2009) 8423–8429.
- [38] S. Kang, M. Herzberg, D.F. Rodrigues, M. Elimelech, Antibacterial effects of carbon nanotubes: size does matter, *Langmuir* 24 (2008) 6409–6413.
- [39] W. Jiang, H. Mashayekhi, B.S. Xing, Bacterial toxicity comparison between nano- and micro-scaled oxide particles, *Environ. Pollut.* 157 (2009) 1619–1625.
- [40] Z.M. Xiu, Q.B. Zhang, H.L. Puppala, V.L. Colvin, P.J.J. Alvarez, Negligible particle-specific antibacterial activity of silver nanoparticles, *Nano Lett.* 12 (2012) 4271–4275.
- [41] W.K. Jung, H.C. Koo, K.W. Kim, S. Shin, S.H. Kim, Y.H. Park, Antibacterial activity and mechanism of action of the silver ion in *Staphylococcus aureus* and *Escherichia coli*, *Appl. Environ. Microbiol.* 74 (2008) 2171–2178.
- [42] Q.L. Feng, J. Wu, G.Q. Chen, F.Z. Cui, T.N. Kim, J.O. Kim, A mechanistic study of the antibacterial effect of silver ions on *Escherichia coli* and *Staphylococcus aureus*, *J. Biomed. Mater. Res.* 52 (2000) 662–668.
- [43] G. Gosheger, J. Hardes, H. Ahrens, A. Streitburger, H. Buerger, M. Erren, A. Günsel, F.H. Kemper, W. Winkelmann, C. von Eiff, Silver-coated megaendoprotheses in a rabbit model – an analysis of the infection rate and toxicological side effects, *Biomaterials* 25 (2004) 5547–5556.
- [44] I. Noda, F. Miyaji, Y. Ando, H. Miyamoto, T. Shimazaki, Y. Yonekura, M. Miyazaki, M. Mawatari, T. Hotokebuchi, Next generation antibacterial hydroxyapatite coating: antibacterial activity of Ag ions in serum, *Bioceram. Dev. Appl.* 1 (2010) 1–3.
- [45] S.L. Zhang, J. Li, G. Lykotrafitis, G. Bao, S. Suresh, Size-dependent endocytosis of nanoparticles, *Adv. Mater.* 21 (2009) 419–424.
- [46] W. Jiang, B.Y.S. Kim, J.T. Rutka, W.C.W. Chan, Nanoparticle-mediated cellular response is size-dependent, *Nat. Nanotechnol.* 3 (2008) 145–150.
- [47] A. Al-Kattan, P. Dufour, J. Dexpert-Ghys, C. Drouet, Preparation and physicochemical characteristics of luminescent apatite-based colloids, *J. Phys. Chem. C* 114 (2010) 2918–2924.
- [48] M. Jelinek, T. Kocourek, K. Jurek, J. Remsa, J. Mikovsky, M. Weiserova, J. Strnad, T. Luxbacher, Antibacterial properties of Ag-doped hydroxyapatite layers prepared by PLD method, *Appl. Phys. A Mater. Sci. Process.* 101 (2010) 615–620.
- [49] H. Vik, K.J. Andersen, K. Julshamn, K. Todnem, Neuropathy caused by silver absorption from arthroplasty cement, *Lancet* 1 (1985) 872.